


EXPRESS LETTER

Open Access



First report of geo- and thermochronological results from the Cordillera Central, Luzon, Philippines

Toru Nakajima^{1*} , Shigeru Sueoka¹, Mitsuhiro Nagata¹, Barry P. Kohn², Noelynna T. Ramos³, Hiroyuki Tsutsumi⁴ and Takahiro Tagami⁵

Abstract

Geo- and thermochronological methods were applied to diorites from the Cordillera Central, Luzon, Philippines to understand their emplacement and exhumation history in the island arc mountains. Five zircon U–Pb ages range from 32.54 ± 0.70 to 6.11 ± 0.15 (2SE) Ma, indicating that dioritic magmas intruded the upper crust intermittently during Cenozoic magmatism. Five zircon fission-track (ZFT) pooled ages range from 35.63 ± 2.17 to 6.91 ± 0.36 (2SE) Ma and are generally comparable with the U–Pb ages at each locality. These results suggest that the diorites cooled rapidly below ~ 250 – 350 °C (i.e., through the partial annealing zone of the ZFT system), following their intrusion. On the other hand, two zircon and five apatite U–Th(–Sm)/He (ZHe and AHe) weighted mean ages, ranging from 11.71 ± 0.36 to 8.82 ± 0.26 and 9.21 ± 0.52 to 0.98 ± 0.09 (2SE) Ma, respectively, indicate a decrease in cooling rates at a lower temperature range, especially through the partial retention zone of the AHe system. This observation suggests that the ZFT ages reflect initial cooling of the dioritic magma, whereas the AHe ages reflect the cooling history associated with regional exhumation following the initial cooling phase. The spatial distribution of the AHe ages suggests that rapid exhumation of the Cordillera Central during the Quaternary resulted from the block-like uplift of the entire mountain range.

Keywords Geochronology, Thermochronology, Arc–Trench system, The Cordillera Central, Exhumation

*Correspondence:

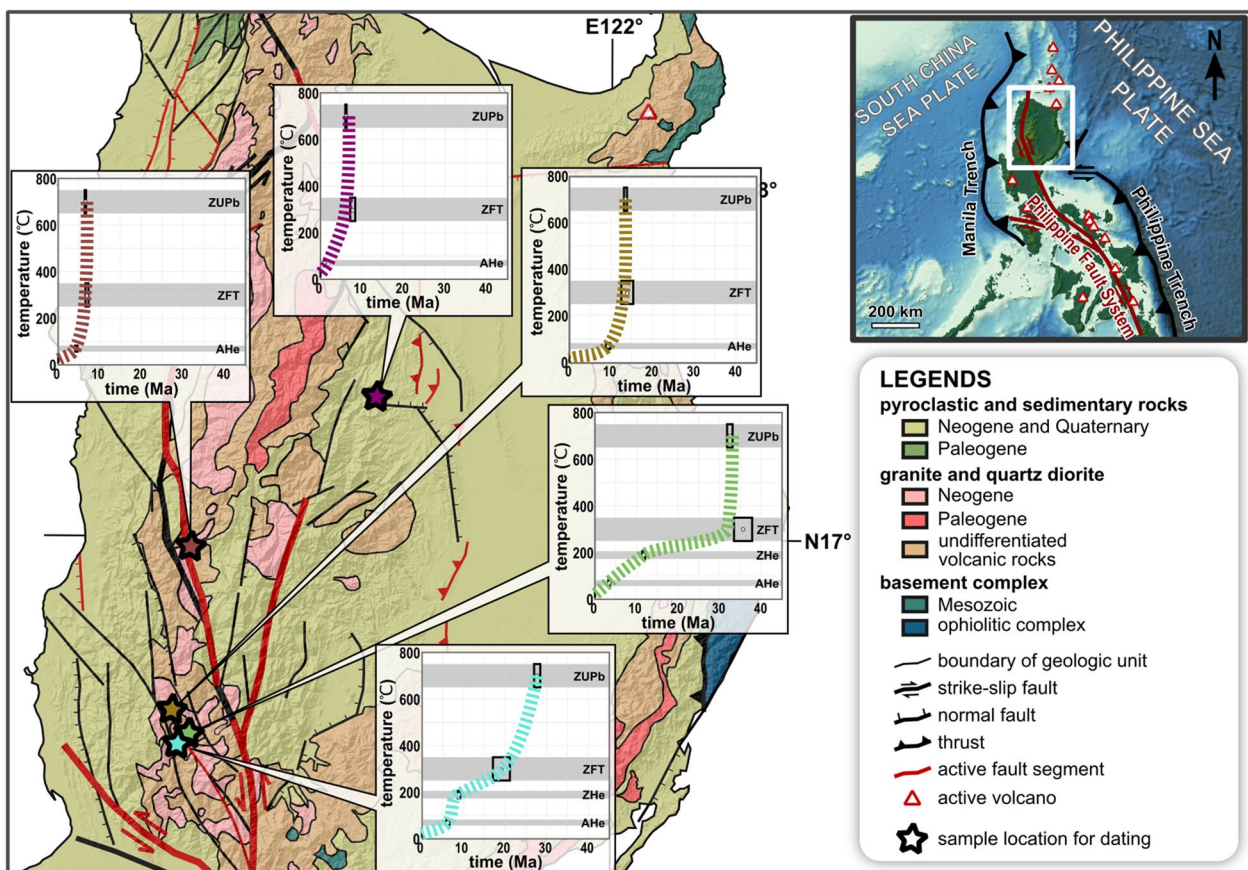
Toru Nakajima
nakajima.toru@jaea.go.jp

Full list of author information is available at the end of the article



© The Author(s) 2023. **Open Access** This article is licensed under a Creative Commons Attribution 4.0 International License, which permits use, sharing, adaptation, distribution and reproduction in any medium or format, as long as you give appropriate credit to the original author(s) and the source, provide a link to the Creative Commons licence, and indicate if changes were made. The images or other third party material in this article are included in the article's Creative Commons licence, unless indicated otherwise in a credit line to the material. If material is not included in the article's Creative Commons licence and your intended use is not permitted by statutory regulation or exceeds the permitted use, you will need to obtain permission directly from the copyright holder. To view a copy of this licence, visit <http://creativecommons.org/licenses/by/4.0/>.

Graphical abstract



Introduction

Investigating the mechanisms of mountain building in arc–trench systems is considered to be important for a more complete understanding of strain buildup and release in island arc interiors (e.g., Ikeda 1996, 2014). Thermochronological methods are commonly employed to constrain the exhumation rate by elucidating the thermal evolution of rocks and their cooling history. Recent thermochronological studies have shed light on the inelastic strain buildup mechanisms associated with the vertical displacement of island arc mountain ranges on geologic timescales (e.g., Sueoka and Tagami 2019). On the other hand, thermochronological studies in island arc mountain ranges are inconclusive and have been concentrated in a limited number of regions (e.g., Northeastern Japan arc: Sueoka et al. 2017b; Fukuda et al. 2019, 2020, Japan Alps: Yamada and Harayama 1999; Ito and Tanaka 1999; Sueoka et al. 2012, 2017a; Spencer et al. 2019; King et al. 2022). Therefore, it is necessary to apply thermochronology studies to mountainous areas in different

island arcs to develop a more comprehensive picture of their evolution.

The Cordillera Central (CC) is a 300-km-long north–south trending mountain range in northern Luzon Island, Philippines (Fig. 1a), which corresponds to a magmatic arc that resulted from subduction along the Manila Trench since the late Oligocene (Fig. 1b; Bellon and Yumul 2000; Queaño et al. 2007). The CC exhibits unique geological features, such as the double subduction of the Philippine Sea plate and the South China Sea plate and large-scale strike-slip faulting (Philippine Fault System) that accommodates the lateral oblique motion of the Philippine Sea plate (Fitch 1972). Nevertheless, modern thermochronological approaches have rarely been applied to the CC. In this study, we report geo- and thermochronological data from diorite samples collected from the CC and briefly discuss its exhumation history. The young zircon U–Pb and fission-track (FT) ages obtained in this study indicate the intermittent intrusion and rapid cooling of dioritic magma since the Oligocene.

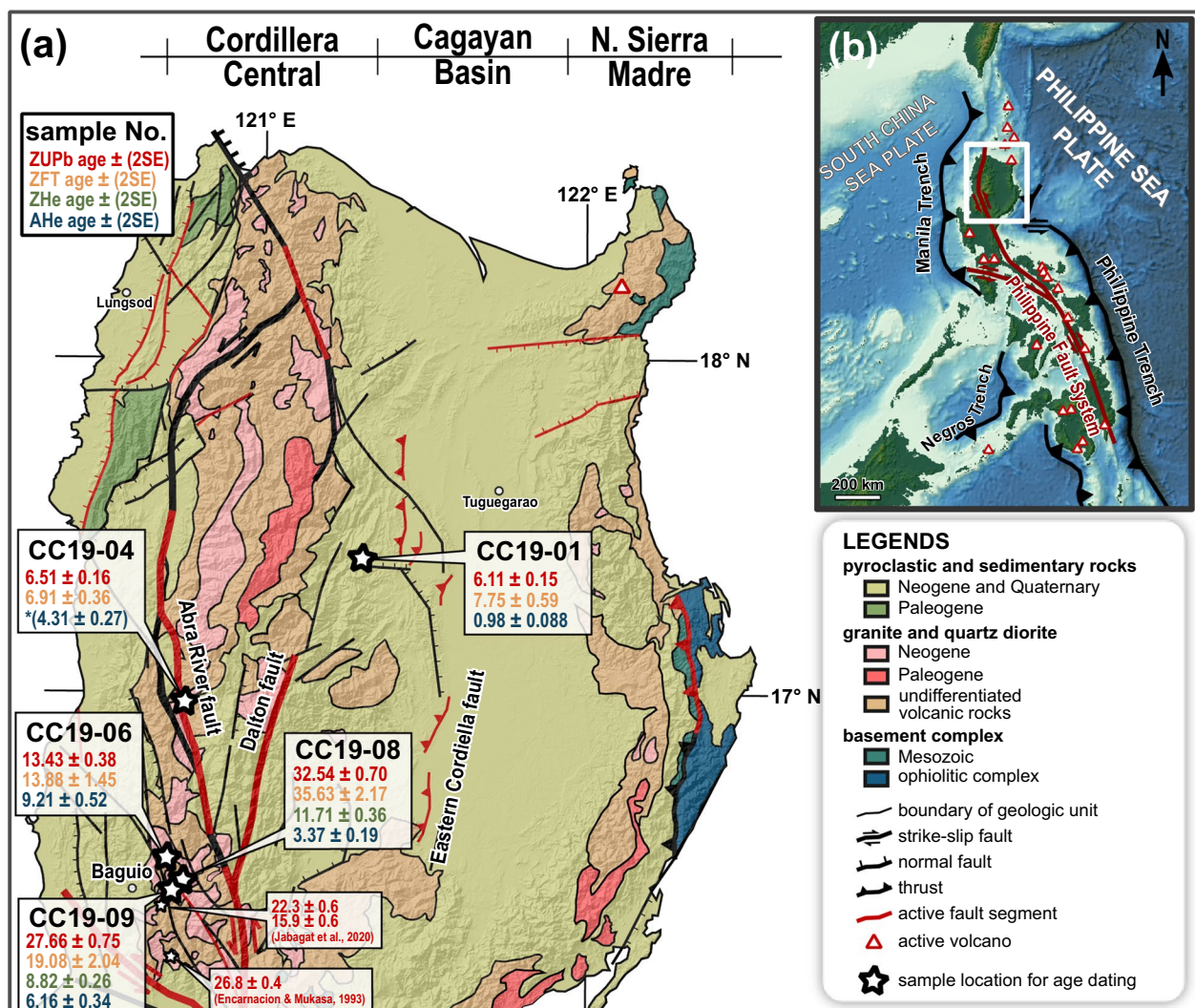


Fig. 1 **a** Geological map of northern Luzon island modified after Geological Survey Division (1963). Stars indicate sample locations for geo- and thermochronological dating. Location of active volcanoes and active faults are based on the PHIVOLCS's reports (DOST-PHIVOLCS 2020). The digital elevation model AW3D30 was obtained from the ALOS/PRISM, Japan Aerospace Exploration Agency. **b** Digital elevation model image of the Philippines with the location of Fig. 1a. The digital elevation model (ETOPO2022) was obtained from the NOAA National Centers for Environmental Information. *The youngest single-grain age is given as a reference. This sample was excluded from the cooling history discussion because of the large dispersion of AHe grain ages and absence of a young age group (detailed in the result section in the main text)

Young U-Th-(Sm)/He ages indicate high Quaternary exhumation rates for the CC. The dataset presented herein contributes important chronological constraints for elucidating the mechanism of CC formation and evolution, which may be relevant to understanding mountain formation in other island arc settings. Moreover, these geo- and thermochronological data are expected to be essential information for regional geological investigations concerning local or regional fault movement, concurrent tectonic block uplift, and the development of sedimentary basins on Luzon Island.

Geological background

The geological and tectonic structure of Luzon Island is a product of the eastward subduction of the South China Sea plate along the Manila Trench and the westward subduction of the Philippine Sea plate along the Philippine Trench (Queaño et al. 2007: Fig. 1b). Two active volcanic fronts are recognized in Luzon Island at present, resulting from arc magmatism and volcanism associated with the oppositely dipping subduction zones, and CC is located in the non-volcanic zone between them. Based on the distribution of igneous

Table 1 Summary of rock samples and result of age determinations

Sample No	E. lon. (deg.)	N. Lat. (deg.)	elev. (m)	a rock type	b zircon U–Pb		c zircon FT		d zircon (U–Th)/He		e apatite (U–Th–Sm)/He					
					n	age (Ma)	n	2SE	n	age (Ma)	n	2SE	n	age (Ma)	2SE	
CC19-01	121.2990	17.4075	353	biotite hornblende diorite	25	6.11	23	0.15	23	7.75	0.59	–	–	5	0.98	0.09
CC19-04	120.7472	16.9820	524	hornblende diorite	25	6.51	35	0.16	35	6.91	0.36	–	–	4	^e (4.31)	(0.27)
CC19-06	120.6909	16.5175	1685	porphyritic hornblende diorite	23	13.4	19	0.38	19	13.88	1.45	–	–	5	9.21	0.52
CC19-08	120.7406	16.4498	668	biotite hornblende granodiorite	25	32.5	32	0.70	32	35.63	2.17	4	11.7	5	3.37	0.19
CC19-09	120.7071	16.4197	965	biotite hornblende diorite	25	27.7	32	0.75	32	19.08	2.04	5	8.82	5	6.16	0.34

Methods and results are detailed in a—Additional file 1 A; b—Additional file 1 B; c—Additional file 1 C; d—Additional file 1 D; e: The youngest single-grain age is given as a reference. This sample was excluded from the cooling history discussion because of the large dispersion of particle ages and absence of young age group (detailed in the result section in the main text)

rocks, the CC is considered to be located on the Oligocene–Miocene volcanic front.

The basement rocks of the CC are composed mainly of Mesozoic meta-volcanic rocks and ophiolites (Ringebach 1992). Basement rocks are exposed in a limited area, and most of the area is covered by Cenozoic volcanic and sedimentary rocks (Fig. 1a). The Cenozoic sedimentary rocks exposed in the CC include the following formations: Pugo Formation, Malitap Formation, Sagada Formation, Zigzag Formation, Kennon Limestone, Klondyke Formation, Mirador Limestone, Baguio Formation, and Malaya Formation (Aurelio and Peña, 2010). These sedimentary rocks are intruded by Cenozoic diorites and interfingering with Quaternary (or age-unknown) volcanic rocks. Three main generations of dioritic bodies have been recognized in the CC region: the Central Cordillera Diorite Complex (late Oligocene), the Itogon Quartz Diorite (early to middle Miocene), and the Black Mountain Quartz Diorite (late Miocene) (Balce 1980; Yumul 1992; Knittel et al. 1995). K–Ar data indicate that these are mostly cooling ages (Wolfe 1981; Sillitoe and Angeles 1985; Maletterre 1989; Imai 2002). As for zircon U–Pb data, only one site

from the Central Cordillera Diorite Complex and some dioritic vein have so far been reported (26.8 ± 0.4 Ma: Encarnacion and Mukasa 1993; 22.3 ± 0.6 Ma and 15.9 ± 0.6 Ma: Jabagat et al. 2020). Geochronological study of these plutonic rocks has been mainly carried out only in the Baguio region in the southern CC (Fig. 1a), and the intrusion age of quartz diorites widely exposed in the CC is still uncertain.

Large-scale left-lateral strike-slip faults traverse the CC. These faults are active segments of the Philippine Fault System, which extends ~1250 km from north to south and is the major structure in this area (Fig. 1b). In the CC, the Philippine Fault System has been active since the Middle Miocene to the present (e.g., Ringebach et al. 1990). Two major segments, the Abra River Fault (ARF) and the Dalton Fault (DF), are recognized in the study area (Fig. 1a), with associated minor branching faults and extensional duplexes (Ringebach et al. 1990). These faults are interpreted as having been activated as strike-slip and thrust faults under a transpressive regime, whereas previous studies also suggest that the regional stress varied over geologic time (Ringebach et al. 1990).

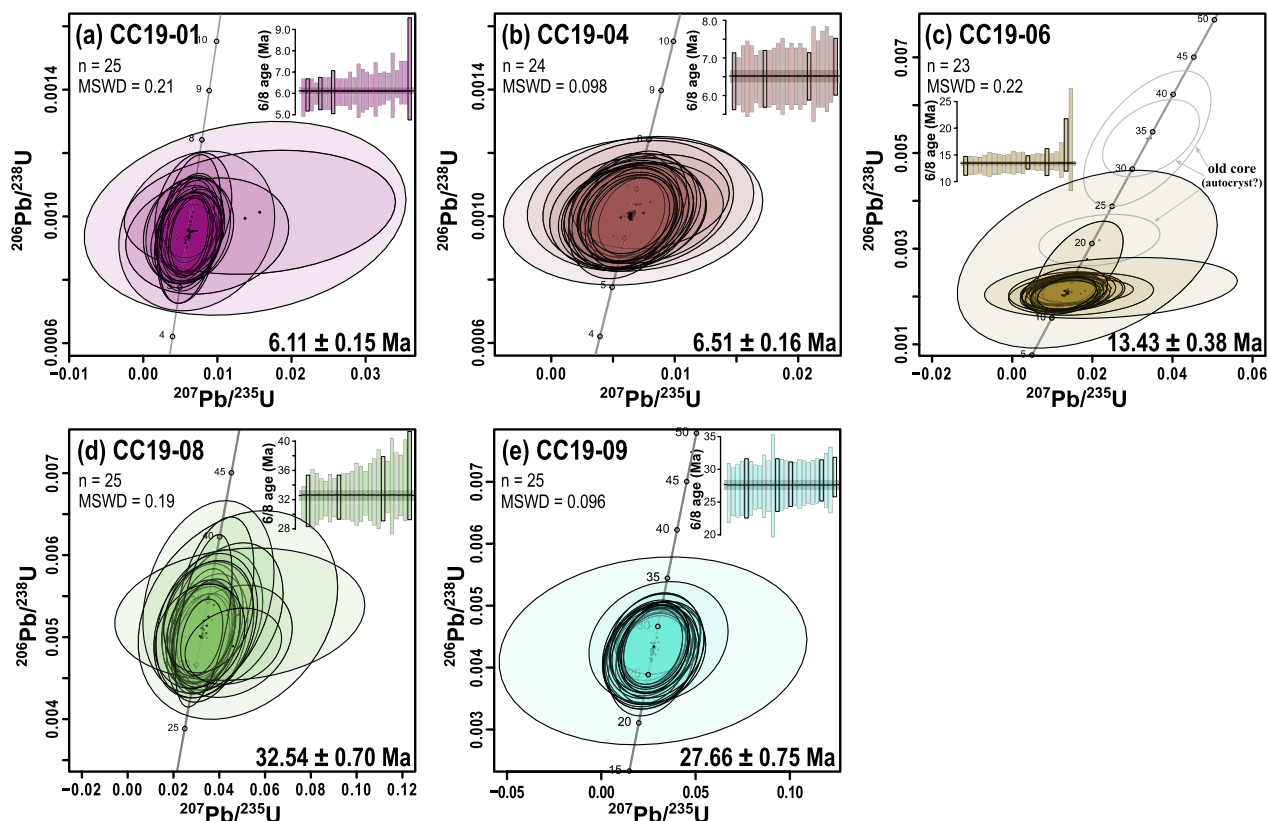


Fig. 2 Zircon U–Pb data plotted on Tera-Wasserburg diagrams and age plot diagram produced using IsoplotR (Vermeesch 2018). $^{206}\text{Pb}/^{238}\text{U}$ weighted mean ages (2σ errors) are shown in the bottom right of each diagram

Methodology

This study selected Cenozoic diorites widely distributed in CC for geo- and thermochronological dating. In general, plutonic rocks exposed in a mountain range are expected to record the exhumation process from emplacement to exposure. They are also useful for geo- and thermochronological studies because they often contain abundant zircon and apatite grains. Five samples of quartz diorite and porphyritic diorite (Table 1) were collected from outcrops in the CC (Fig. 1a). Petrographic descriptions of each sample are presented in Additional file 1A. Samples were crushed, and zircon and apatite grains were separated using standard heavy liquid techniques at Kyoto Fission-Track Co., Ltd., Japan.

Separated apatite and zircon fractions were distributed to two laboratories: Tono Geoscience Center (Japan) for zircon U–Pb and fission-track (FT) dating, and the University of Melbourne (Australia) for zircon and apatite U–Th-(Sm)/He dating. Detailed dating methods employed are summarized in Additional file 1B–D. Although preliminary apatite FT measurements were conducted, a large number of dislocations were observed in the mounted and etched apatite grains (Additional file 1: Fig. S-C2) making them unsuitable for further study.

Results of geo- and thermochronological dating

Zircon U–Pb ages

The U–Pb data obtained in this study are shown in Fig. 2 and detailed in Additional file 1: Table S-B2–7. Twenty-six measurements were taken for each sample, including the geometric core and rim of zircons. At almost all points of measurement, the $^{206}\text{Pb}/^{238}\text{U}$ – $^{207}\text{Pb}/^{235}\text{U}$ ratio was concordant in the range between 97 and 103%, and a representative U–Pb age was calculated as the weighted average of the $^{206}\text{Pb}/^{238}\text{U}$ ages without any common Pb correction. Points that corresponded to any of the following two cases were excluded from the age calculations: (1) where mineral inclusions were clearly considered to be ablated on the basis of a signal change over time, and (2) the $^{206}\text{Pb}/^{238}\text{U}$ – $^{207}\text{Pb}/^{235}\text{U}$ ratio was discordant in the range between 97 and 103%. All analyses yield well-defined single-population ages of 6.11 ± 0.15 Ma, 6.51 ± 0.16 Ma, 13.43 ± 0.38 Ma, 32.54 ± 0.70 , and 27.66 ± 0.75 Ma for samples CC19-01, CC19-04, CC19-06, CC19-08, and CC19-09, respectively (2SE). No significant age differences are recognized between the geometric core and rims of zircons in any of the samples which exhibit oscillatory zoning (Additional file 1: Fig. S-B3–7). Significantly, older data were obtained from the core of three grains in sample CC19-06 (spots. 14, 15, and 16: Additional file 1: table S2 and Fig. S-B3). These three data did not overlap

with the all-in weighted average in the error range (2SD) and therefore were excluded from the weighted average $^{206}\text{Pb}/^{238}\text{U}$ age calculation.

Zircon fission-track age

The zircon fission-track (ZFT) grain ages obtained exhibit a unimodal Poisson distribution (Additional file 1: Fig. S-C1). Since multiple components were not clearly detected despite the large dispersion of grain ages, the FT age was calculated as the pooled age (Hasebe et al. 2013): 7.75 ± 0.59 Ma, 6.91 ± 0.36 Ma, 13.88 ± 1.45 Ma, 35.63 ± 2.17 Ma, and 19.08 ± 2.04 Ma for samples CC19-01, CC19-04, CC19-06, CC19-08, and CC19-09, respectively (2SE). Detailed results are summarized in Additional file 1: Table S-C1–6. Confined ZFT track lengths were not measured as only a limited number of zircon grains could be separated from samples.

Zircon and apatite U–Th-(Sm)/He age

In this study, U–Th-(Sm)/He dating was performed on five grains for each sample. Representative age values for each sample were derived from the weighted average of the grain ages. In cases where intra-sample grain ages were significant (Additional file 1: Figs. S-D1 and 2), the youngest of the age groups that overlapped within the 2SD range was accepted for calculation of cooling ages, and the older grain ages were excluded. Because there is no clear relationship between grain ages and their effective U concentration, which may result from He diffusion due to the effects of alpha-radiation damage (e.g., Guenther et al. 2013), the observed dispersion of intra-grain ages may possibly be due to the internal zonation of U and Th concentrations, variations in grain size, the existence of small U and/or Th-rich micro-inclusions, grain fragmentation, He-rich fluid inclusions, and crystal defects acting as He traps (e.g., Shuster et al. 2006; Brown et al. 2013; Danišik et al. 2017). Apatite (U–Th–Sm)/He (AHe) cooling age were not calculated for sample CC19-04 because the dispersion of grain ages was significant and age groups were not recognized near the youngest grain age.

Middle Miocene zircon (U–Th)/He (ZHe) ages obtained for CC19-08 and CC19-09 are 11.71 ± 0.36 Ma and 8.82 ± 0.26 Ma, respectively. AHe ages range from Pleistocene to Miocene: 0.98 ± 0.088 Ma, 4.31 ± 0.27 Ma, 9.21 ± 0.52 Ma, 3.37 ± 0.19 Ma, and 6.16 ± 0.34 Ma for samples CC19-01, CC19-04, CC19-06, CC19-08, and CC19-09, respectively (2SE). These ages are significantly

younger than the zircon U–Pb and ZFT ages and their analytical uncertainties obtained from the same samples.

Discussion

Timing of the dioritic magma intrusion

The zircon U–Pb ages reported in this study are interpreted as the age of intrusion of the dioritic magma at each sampling site based on the following observations and measurements: (1) zircons are commonly found as an accessory mineral in the samples; (2) most zircons show no apparent zoning or oscillatory zoning under cathodoluminescence images and no distinct boundaries were observed between geometric core and rims in most grains (Additional file 1: Fig. S-B1); and (3) even where clear core–rim microstructures are observed, no obvious U–Pb age difference is recognized between them (Fig. 2).

Samples CC19-01 and 04 yield an intrusion age of ca. 6–7 Ma, which correlates with the late Miocene Black Mountain Quartz Diorite (Wolfe 1981; Sillitoe and Angeles 1985) in the Baguio region. These U–Pb ages indicate that late Miocene quartz diorite is extensively distributed in the CC although the spatial distribution remains unclear. The U–Pb age of CC19-06 corresponds to the early–middle Miocene Itogon Quartz Diorite (Maletterre 1989; Jabagat et al. 2020), and the CC19-09 is considered to be a correlative of the late Oligocene Central Cordillera Diorite Complex and its syn-effusive rocks, the Zig-zag Formation (Encarnacion and Mukasa 1993; Jabagat et al. 2020). On the other hand, an early Oligocene quartz diorite comparable to CC19-08 has not been reported in the CC. Deposition of the Apaoan Volcaniclastics (Garcia 1991) coincides with the intrusion of the quartz diorite of the CC19-08, suggesting early igneous activity in the CC during early Oligocene time. Quartz diorite sample CC19-08 is also comparable with the northern Sierra Madre batholiths of eastern Luzon Island (Billedo 1994). These zircon U–Pb ages suggest intermittent igneous

activity and associated dioritic magma intrusions from early Oligocene to late Miocene in the CC accompanied by the westward subduction of the West Philippine Basin and the eastward subduction of the South China Sea Plate (Queaño et al. 2007).

Cooling history

The approximate thermal history, i.e., time–temperature path (t – T path), of each sample can be simply determined based on the relationship between multiple age systems and their assumed closure temperatures obtained from a single sample. Strictly speaking, as closure temperatures may vary in relation to mineral grain size and cooling rate, this approach cannot be applied to quantitatively constrain the cooling rate. On the other hand, this approach can contribute to reconstructing an approximate cooling history (Wagner et al. 1977). On the range of cooling rates of 10–100 °C / Myr, closure temperatures are approximated to be ca. 250–350 °C for ZFT (Tagami et al. 1998; Yamada et al. 2007; Ketcham 2019), 183–207 °C for ZHe (Reiners et al. 2004; Guenther et al. 2013), and 67–83 °C for the AHe system (Farley 2000; Flowers et al. 2009), respectively. Since effective U concentrations of zircon and apatite measured in this study are relatively low (zircon: 102.6–572.4 ppm; apatite: 0.9–25.5 ppm), the effects of radiation damage on age dispersion and the possible closure temperature are not considered. Moreover, as mentioned in the previous section, zircon U–Pb ages obtained in this study are interpreted as intrusion ages and are considered to reflect the timing of solidification and cooling below the wet solidus of dioritic magma (650–750 °C: Bea et al. 2021). The surface temperature and topographic lapse rate are set to 25.0 °C and 0.6 °C / km (Naito et al. 2006). The t – T paths constructed by connecting these ages and temperature ranges are shown in Fig. 3.

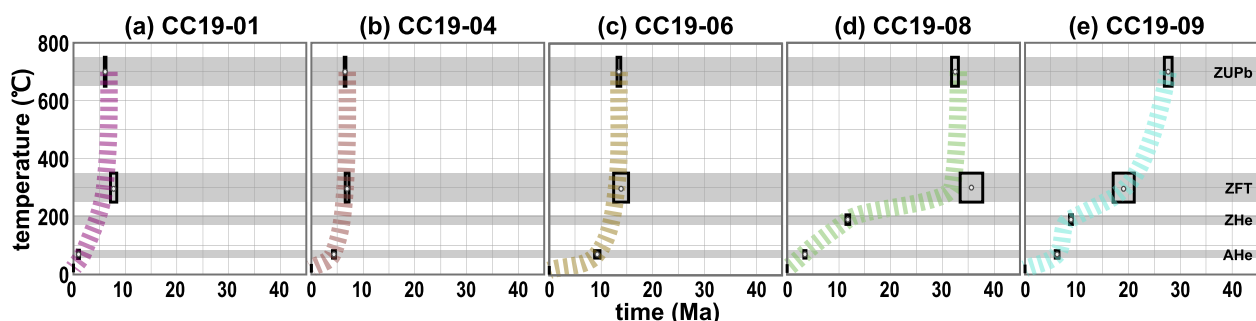


Fig. 3 The approximate thermal history (t – T path: bold broken lines) of each sample. Shaded areas represent a wet-solidus temperature range (for zircon U–Pb) and partial anneal and retention zones of each thermochronometer. Boxes represent a constraint resulting from age determination, and their width corresponds to the errors (2SE). It should be noted that the AHe ages and their errors for CC19-04 are reference values represented by the youngest grain age (4.31 ± 0.27 Ma)

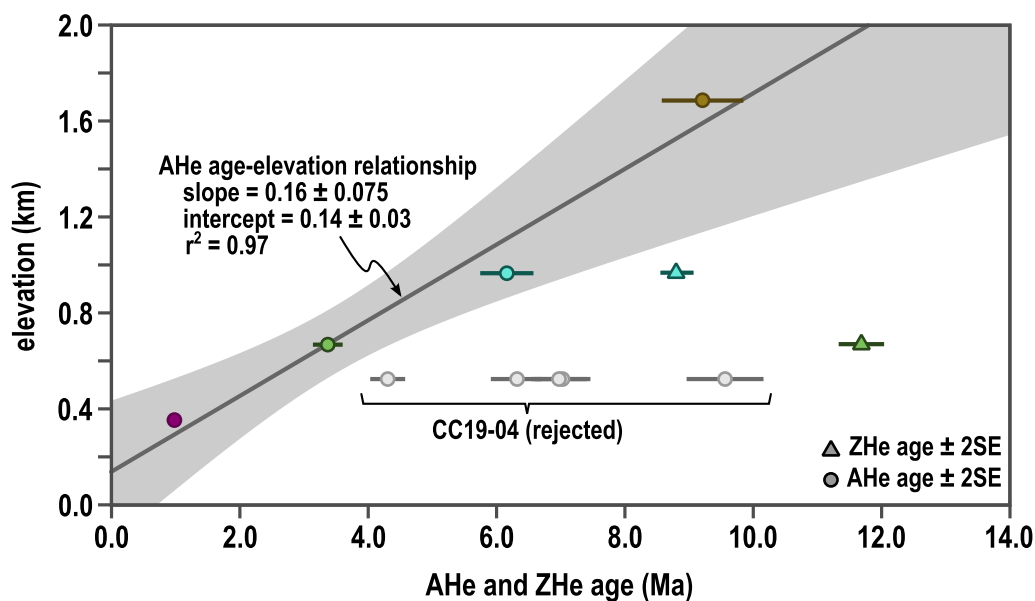


Fig. 4 ZHe and AHe ages plotted against sample elevations. Colors of each point correspond to those of the location in Fig. 1. Line represents an error-weighted least squares linear regression (95% confidence) interval

For samples CC19-01, 04, 06, and 08, zircon U–Pb and FT ages are consistent (excluding sample CC19-09) or rather ZFT ages are older. Zircons in all samples display few inclusions and dislocations and show minimal density zonation of FTs. Hence, the exact reason for the systematic occurrence of older ZFT ages in comparison to the U–Pb ages remains unknown. Regardless of the underlying cause, it is noteworthy that these ZFT ages are close in timing within analytical uncertainties to the U–Pb ages. This suggests that following intrusion and solidification of dioritic magma samples cooled rapidly down to around 250–350 °C, reflecting the crustal thermal background. Following this phase, the cooling rate decreased in all samples at a lower temperature, especially in the range of the AHe closure temperature. This decrease may reflect the transition from initial magmatic cooling post-emplacement to a gradual cooling phase associated with subsequent exhumation. Thus, we interpret ZFT ages as indicating the later stage of initial magmatic cooling of the dioritic magma, whereas the AHe ages reflect their time of later exhumation.

ZHe ages may reflect cooling associated with exhumation, since the cooling rate decreases from ZFT to the ZHe temperature range (Fig. 3) for the two samples (CC19-08 and 09). Nevertheless, for CC19-09, the cooling rate increases from the partial retention zone of ZHe to AHe, while the neighboring sample CC19-08 does not show such behavior. This suggests a possible discontinuity of the thermal structure between the two samples, which may be attributed to either the presence of a fault

or a later thermal event, such as magma intrusion, that could have reset the ZHe system of CC19-09. However, due to the lack of sufficient data, a more detailed discussion is not possible.

Preliminary discussion of exhumation history of the CC

This section provides a preliminary discussion of the exhumation history of the CC based on the spatial distribution of AHe ages, which are interpreted as signifying their exhumation. AHe data for CC19-04 are excluded from this discussion because of the large dispersion of grain ages making it difficult to resolve an age cluster (Fig. 4 and Additional file 1: Fig. S-C1), and outcrop observations suggesting that this sample might be located in the deformation zone of the ARF (Additional file 1 Fig. S-A2).

As shown by the AHe age–elevation relationship in Fig. 4, the AHe shows a linear distribution against elevation (slope=0.16±0.075 km/Ma, r²=0.97). This age distribution can be interpreted as either 1) a linear age distribution reflecting steady-state exhumation or 2) an exhumed partial retention zone. In either case, this age distribution suggests that the geologic body from which samples were collected was exhumed as a single tectonic unit. It should be noted here that rock samples were collected across the eastern and western slopes of the CC and across the eastern and western blocks of the ARF and DF. Hence, this age distribution indicates that the entire CC was uplifted in a block-like manner, regardless of the activity of the ARF and DF in the study area.

Both interpretations of the AHe age distribution mentioned above suggest Quaternary acceleration of the exhumation rate from relatively slow exhumation in Neogene time in the CC. In case 1, the slope of the age–elevation relation suggests an exhumation rate of 0.16 ± 0.075 mm/yr during the Neogene (ca. 10–1 Ma). The positive intercept of the regression line (0.14 km; Fig. 4) indicates a post-Quaternary acceleration of the exhumation rate. In case 2, the age pattern is interpreted as having been formed in the partial retention zone of AHe during a tectonically and thermally stable phase at $> \sim 10$ Ma, which was subsequently exposed by rapid exhumation at $< \sim 1$ Ma (an exhumed partial retention zone). This interpretation provides a different exhumation history before 1 Ma from case 1, while both cases are consistent in suggesting an acceleration of the exhumation rate after 1 Ma. It should be noted that the timing and rate of exhumation acceleration post-1 Ma is debatable, as there is not sufficient thermochronological data to accurately estimate the break point.

If the development of flower structures associated with the activity of the ARF and DT (Ringebach et al. 1990) has a first-order control on the uplift of the CC, then distinct differences in uplift style are expected between the east and west blocks of these faults. This hypothesis is also applicable to segments of the Philippine Fault System other than the ARF and DT; however, the AHe age distribution in this study is not consistent with this model. Thus, the contribution of the fault activity of the ARF and DT to the exhumation of the CC is limited, and a different driving force is required to explain the AHe age distribution. Our data may suggest that active faulting in the frontal thrust of the CC foothills, uplifted the whole belt as a block (e.g., East Cordillera Fault shown in Fig. 1a: DOST-PHIVOLCS 2020).

Conclusions

In this study, geo- and thermochronological dating of five diorite samples collected from the CC were carried out. Zircon U–Pb ages indicate that intermittent igneous activity with associated dioritic intrusions extended from the early Oligocene to the late Miocene. Following intrusion, the diorites cooled rapidly down to the temperature range of partial annealing zone of the ZFT system, followed by gradual cooling accompanied by regional exhumation. The distribution pattern of AHe ages in the study area suggests a pattern of block-like uplift of the CC (between ~ 1 and 10 Ma) marked by Quaternary acceleration of the exhumation rate.

Abbreviations

CC Cordillera Central
ARF Abra River Fault

DF Dalton Fault
ZFT Zircon fission-track
ZHe Zircon (U-Th)/He
AHe Apatite (U-Th-Sm)/He

Supplementary Information

The online version contains supplementary material available at <https://doi.org/10.1186/s40623-023-01927-z>.

Additional file 1.

Acknowledgements

The authors thank two anonymous reviewers for their constructive comments, which greatly improved the manuscript. Zircon and apatite separation was carried out at Kyoto Fission-Track Co., Ltd. by Drs. T. Danhara and H. Iwano. The ^{238}U concentration measurement using LA–ICP–MS was conducted with the cooperation of Dr. S. Kagami from Tono Geoscience Center, Japan Atomic Energy Agency. Field sampling was conducted with assistance from L. Nawanao Jr., L.F. Sarmiento, and A.D. Pamintuan of the National Institute of Geological Sciences at the University of the Philippines. This study was carried out under financial support by Grant-in-Aid for Scientific Research (C) from Japan Society of Promotion of Science (No. 21K03730, representative: Shigeru Sueoka). The University of Melbourne thermochronology laboratories receive support under the AuScope program of the National Collaborative Research Infrastructure Strategy (NCRIS) and operate under the University of Melbourne TrACCESS Research Platform.

Author contributions

TN drafted the manuscript and performed ZFT dating. SS, HT, and TT are responsible for the project and conducting research planning. MN and TN performed zircon U–Pb dating. BK performed ZHe and AHe dating. SS, NR, HT, and TT planned and carried out fieldwork and rock sampling. All the authors read and approved the final manuscript.

Funding

This study was founded by the Grant-in-Aid for Scientific Research (C) from Japan Society of Promotion of Science (No. 21K03730, representative: Shigeru Sueoka).

Availability of data and materials

The data for this paper are presented in the tables and Additional file.

Declarations

Ethics approval and consent to participate

Not applicable

Consent for publication

Not applicable

Competing interests

The authors declare that they have no competing interests.

Author details

¹Tono Geoscience Center, Japan Atomic Energy Agency, Gifu, Japan. ²School of Geography, Earth and Atmospheric Sciences, University of Melbourne, Melbourne, Australia. ³National Institute of Geological Sciences, University of the Philippines Diliman, Quezon City, Philippines. ⁴Department of Environmental Systems Science, Faculty of Science and Engineering, Doshisha University, Kyotanabe, Japan. ⁵Department of Geology and Mineralogy, Graduate School of Science, Kyoto University, Kyoto, Japan.

Received: 2 April 2023 Accepted: 30 October 2023

Published online: 24 November 2023

References

- Aurelio MA, Peña RE (2010) (Eds.) *Geology of the Philippines*, 2nd Edition. Mines and Geoscience Bureau 532 pp.
- Balce GR (1980) Geology of the Baguio district and its implication on the tectonic development of the Luzon Cordillera Central. *Geol Paleontol Southeast Asia* 21:265–288
- Bea F, Morales I, Molina JF et al (2021) Zircon stability grids in crustal partial melts: implications for zircon inheritance. *Contrib to Mineral Petrol* 176(3):1–13. <https://doi.org/10.1007/S00410-021-01772-X>
- Bellon H, Yumul P Jr, G, (2000) Mio-Pliocene magmatism in the Baguio Mining District (Luzon, Philippines): age clues to its geodynamic setting. *Comptes Rendus L'Académie Des Sci - Ser IIA - Earth Planet Sci* 331:295–302. [https://doi.org/10.1016/S1251-8050\(00\)01415-4](https://doi.org/10.1016/S1251-8050(00)01415-4)
- Billedo EB (1994) *Geologie de la Sierra Madre septentrionale et de l'archipel de Polillo (central Mobile Est Philippine): implications géodynamiques*. University of Nice-Sophia Antipolis
- Brown RW, R. Beucher R, Roper S, Persano C, Stuart F, Fitzgerald P, (2013) Natural age dispersion arising from the analysis of broken crystals. Part I: theoretical basis and implications for the apatite (U–Th)/He thermochronometer. *Geochim Cosmochim Acta* 122:478–497
- Danišik M, McInnes BI, Kirkland CL, McDonald BJ, Evans NJ, Becker T (2017) Seeing is believing: visualization of He distribution in zircon and implications for thermal history reconstruction on single crystals. *Sci Adv* 3(2):e1601121
- DOST-PHIVOLCS (2020) Distribution of Active Faults and Trenches in the Philippines. <https://www.phivolcs.dost.gov.ph/index.php/earthquake/earthquake-generators-of-the-philippines>
- Encarnacion PJ, Mukasa BS (1993) Zircon U–Pb Geochronology of the Zambales and Angat Ophiolites, Luzon, Philippines. *J Geophys Res* 98:19991–20004. <https://doi.org/10.1029/93JB02167>
- Farley KA (2000) Helium diffusion from apatite: General behavior as illustrated by Durango fluorapatite. *J Geophys Res Solid Earth* 105:2903–2914. <https://doi.org/10.1029/1999jb900348>
- Fitch TJ (1972) Plate convergence, transcurrent faults, and internal deformation adjacent to Southeast Asia and the western Pacific. *J Geophys Res* 77:4432–4460. <https://doi.org/10.1029/JB077i023P04432>
- Flowers RM, Ketcham RA, Shuster DL, Farley KA (2009) Apatite (U–Th)/He thermochronometry using a radiation damage accumulation and annealing model. *Geochim Cosmochim Acta* 73:2347–2365. <https://doi.org/10.1016/J.GCA.2009.01.015>
- Fukuda S, Sueoka S, Hasebe N et al (2019) Thermal history analysis of granitic rocks in an arc-trench system based on apatite fission-track thermochronology: A case study of the Northeast Japan Arc. *J Asian Earth Sci* X 1:100005. <https://doi.org/10.1016/j.jaesx.2019.100005>
- Fukuda S, Sueoka S, Kohn BP, Tagami T (2020) (U–Th)/He thermochronometric mapping across the northeast Japan Arc: towards understanding mountain building in an island-arc setting. *Earth Planet Space*. <https://doi.org/10.1186/s40623-020-01151-z>
- Garcia JS (1991) Geology and mineralization characteristics of the Mankayan Mineral district, Bunguet, Philippines. *Geol Soc Japan Rep* 277:21–30
- Geological Survey Division P (1963) *Geological map of the Philippines*, 1st edn. Bureau of Mines, in coordination with the Board of Technical Surveys and Maps
- Guenther WR, Reiners PW, Ketcham RA et al (2013) Helium diffusion in natural zircon: radiation damage, anisotropy, and the interpretation of zircon (U–Th)/He thermochronology. *Am J Sci* 313:145–198. <https://doi.org/10.2475/03.2013.01>
- Hasebe N, Tamura A, Arai S (2013) Zeta equivalent fission-track dating using LA-ICP-MS and examples with simultaneous U–Pb dating. *Isl Arc* 22:280–291. <https://doi.org/10.1111/iar.12040>
- Ikeda Y (1996) Implications of active fault study for the present-day tectonics of the Japan arc. *Acta Fault Res* 15:93–99. https://doi.org/10.11462/af1985.1996.15_93
- Ikeda Y (2014) Strain buildup in the Northeast Japan orogen with implications for gigantic subduction earthquakes. *Episodes* 37:234–245. <https://doi.org/10.18814/EPIIUGS/2014/V37i4/003>
- Imai A (2002) Metallogenesis of porphyry Cu deposits of the western Luzon arc, Philippines: K–Ar ages, SO₃ contents of microphenocrystic apatite and significance of intrusive rocks. *Resour Geol* 52:147–161. <https://doi.org/10.1111/j.1751-3928.2002.tb00127.x>
- Ito H, Tanaka K (1999) Radiometric age determination on some granitic rocks in the Hida range, central Japan: remarkable age difference across a fault. *地質学雑誌* 105:241–246. <https://doi.org/10.5575/GEOSOC.105.241>
- Jabagat KD, Gabo-Ratio JA, Queaño KL, Yonezu K, Dimalanta CB, Lee YH, Yumul GP Jr (2020) Petrogenetic constraints on magma fertility in the Baguio mineral district, Philippines: Probing the mineralization potential of the igneous host rocks in the Sangilo epithermal deposit. *Ore Geol Rev* 125:103703. <https://doi.org/10.1016/j.oregeorev.2020.103703>
- Ketcham RA (2019) *Fission-track annealing: from geologic observations to thermal history modeling*. Springer, Cham, pp 49–75
- King GE, Ahadi F, Sueoka S et al (2022) Eustatic change modulates exhumation in the Japanese Alps. *Geology*. <https://doi.org/10.1130/G50599.1>
- Knittel U, Trudu AG, Winter W et al (1995) Volcanism above a subducted extinct spreading center: a reconnaissance study of the North Luzon Segment of the Taiwan-Luzon Volcanic Arc (Philippines). *J Southeast Asian Earth Sci* 11:95–109. [https://doi.org/10.1016/0743-9547\(94\)00039-H](https://doi.org/10.1016/0743-9547(94)00039-H)
- Maletterre P (1989) *Histoire sédimentaire, magmatique, tectonique et métallogénique d'un arc cenozoïque déformé en régime de transpression: la Cordillère Centrale de Luzon, à l'extrémité de la faille philippine, sur les transectes de Baguio et de Cervantes-Bontoc: contexte*. Université de Bretagne Occidentale, Brest
- Naito N, Ageta Y, Iwata S et al (2006) Glacier shrinkages and climate conditions around Jichu Dramo Glacier in the Bhutan Himalayas from 1998 to 2003. *Bull Glaciol Res* 23:51–61
- Queaño KL, Ali JR, Milsom J et al (2007) North Luzon and the Philippine Sea Plate motion model: insights following paleomagnetic, structural, and age-dating investigations. *J Geophys Res Solid Earth* 112:B05101. <https://doi.org/10.1029/2006JB004506>
- Reiners PW, Spell TL, Nicolescu S, Zanetti KA (2004) Zircon (U–Th)/He thermochronometry: He diffusion and comparisons with ⁴⁰Ar/³⁹Ar dating. *Geochim Cosmochim Acta* 68:1857–1887. <https://doi.org/10.1016/j.gca.2003.10.021>
- Ringenbach CJ, Stephan FJ, Maletterre P, Bellon H (1990) Structure and geological history of the Lepanto-Cervantes releasing bend on the Abra River Fault, Luzon Central Cordillera, Philippines. *Tectonophysics* 183:225–241. [https://doi.org/10.1016/0040-1951\(90\)90418-8](https://doi.org/10.1016/0040-1951(90)90418-8)
- Ringenbach CJ (1992) *La Faille Philippine et les chaînes en décrochement associées (center et nord de Luzon): Evolution Cenozoïque et cinématique des déformations quaternaires*. PhD Thesis University de Nice Sophia Antipolis
- Shuster DL, Flowers RM, Farley KA (2006) The influence of natural radiation damage on helium diffusion kinetics in apatite. *Earth Planet Sci Lett* 249:148–161
- Sillitoe RH, Angeles CA (1985) Geological characteristics and evolution of a gold-rich porphyry copper deposit at Guinaoang, Luzon, Philippines. *Asian Min '85*, London, Instn, Min Met 15–26
- Spencer CJ, Danišik M, Ito H et al (2019) Rapid exhumation of earth's youngest exposed granites driven by subduction of an oceanic arc. *Geophys Res Lett* 46:1259–1267. <https://doi.org/10.1029/2018GL080579>
- Sueoka S, Tagami T (2019) Low-temperature thermochronology and its application to tectonics in the shallow crust. *J Geogr* 128:707–730. <https://doi.org/10.5026/jgeography.128.707>
- Sueoka S, Kohn BP, Tagami T et al (2012) Denudation history of the Kiso Range, central Japan, and its tectonic implications: Constraints from low-temperature thermochronology. *Isl Arc* 21:32–52. <https://doi.org/10.1111/j.1440-1738.2011.00789.x>
- Sueoka S, Ikeda Y, Kano K et al (2017a) Uplift and denudation history of the Akaishi range, a thrust block formed by arc-arc collision in central Japan: Insights from low-temperature thermochronometry and thermokinematic modeling. *J Geophys Res Solid Earth* 122:6787–6810. <https://doi.org/10.1002/2017JB014320>
- Sueoka S, Tagami T, Kohn BP (2017b) First report of (U–Th)/He thermochronometric data across Northeast Japan arc implications for the long-term inelastic deformation crustal dynamics: unified understanding of geodynamics processes at different time and length scales Yoshihisa Iio, Richard. *Earth Planet Sp* 69. <https://doi.org/10.1186/s40623-017-0661-z>
- Tagami T, Galbraith RF, Yamada R, Laslett GM (1998) Revised annealing kinetics of fission tracks in zircon and geological implications. In: van den Haute P, de Corte F (eds) *Advances in fission-track geochronology*. Springer, Netherlands, pp 99–112

- Vermeesch P (2018) Geoscience frontiers IsoplotR: a free and open toolbox for geochronology. *Geosci Front* 9:1479–1493. <https://doi.org/10.1016/j.gsf.2018.04.001>
- Wagner GA, Reimer G, Jäger E (1977) Cooling ages derived by apatite fission-track, mica Rb-Sr and K-Ar dating; the uplift and cooling history of the Central Alps. *Mem Inst Geol Miner Univ Padova* 30:1–27
- Wolfe JA (1981) Philippine geochronology. *J Geol Soc Philipp* 35:1–30
- Yamada R, Harayama S (1999) Fission track and K-Ar dating on some granitic rocks of the Hida mountain range, Central Japan. *Geochem J* 33:59–66. <https://doi.org/10.2343/GEOCHEM.33.59>
- Yamada R, Murakami M, Tagami T (2007) Statistical modelling of annealing kinetics of fission tracks in zircon; reassessment of laboratory experiments. *Chem Geol* 236:75–91. <https://doi.org/10.1016/j.chemgeo.2006.09.002>
- Yumul GP (1992) Preliminary geochemical evidences for a marginal basin basement complex for the Baguio mining district, Luzon, Philippines. *J Geol Soc Philipp* 47:5–16

Publisher's Note

Springer Nature remains neutral with regard to jurisdictional claims in published maps and institutional affiliations.

Submit your manuscript to a SpringerOpen[®] journal and benefit from:

- ▶ Convenient online submission
- ▶ Rigorous peer review
- ▶ Open access: articles freely available online
- ▶ High visibility within the field
- ▶ Retaining the copyright to your article

Submit your next manuscript at ▶ [springeropen.com](https://www.springeropen.com)
